

# 1 Application of regional meteorology and air quality models 2 based on MIPS and LoongArch CPU Platforms

3  
4 Zehua Bai<sup>1,2</sup>, Qizhong Wu<sup>1,2</sup>, Kai Cao<sup>1,2</sup>, Yiming Sun<sup>3</sup>, Huaqiong Cheng<sup>1,2</sup>

5  
6 <sup>1</sup>College of Global Change and Earth System Science, Faculty of Geographical Science,  
7 Beijing Normal University, Beijing 100875, China.

8 <sup>2</sup>Joint Center for Earth System Modeling and High Performance Computing, Beijing  
9 Normal University, Beijing 100875, China.

10 <sup>3</sup>Beijing Institute of Talent Development Strategy, Beijing 100032, China.

11  
12 **Correspondence:** Qizhong Wu ([wqizhong@bnu.edu.cn](mailto:wqizhong@bnu.edu.cn))

13  
14 **Abstract.** The Microprocessor without interlocked piped stages (MIPS) and  
15 LoongArch are Reduced Instruction Set Computing (RISC) processor architectures,  
16 which have advantages in terms of energy consumption and efficiency. There are few  
17 studies on the application of MIPS and LoongArch CPUs in the geoscientific numerical  
18 models. In this study, Loongson 3A4000 CPU platform with MIPS64 architecture and  
19 Loongson 3A6000 CPU platform with LoongArch architecture were used to establish  
20 the runtime environment for the air quality modelling system Weather Research and  
21 Forecasting–Comprehensive Air Quality Model with extensions (WRF-CAMx), in  
22 Beijing-Tianjin-Hebei region. The results show that the relative errors for the major  
23 species (NO<sub>2</sub>, SO<sub>2</sub>, O<sub>3</sub>, CO, PNO<sub>3</sub> and PSO<sub>4</sub>) between the MIPS and X86 benchmark  
24 platform are within ±0.1%. The maximum Mean Absolute Error (MAE) of major  
25 species ranged to 10<sup>-2</sup> ppbV or μg m<sup>-3</sup>, the maximum Root Mean Square Error (RMSE)  
26 ranged to 10<sup>-1</sup> ppbV or μg m<sup>-3</sup>, and the Mean Absolute Percentage Error (MAPE)  
27 remained within 0.5%. The CAMx takes about 195 minutes on Loongson 3A4000 CPU,  
28 71 minutes on Loongson 3A6000 CPU and 66 minutes on Intel Xeon E5-2697 v4 CPU,  
29 when simulating a 24h-case with four parallel processes using MPICH. As a result, the

删除的内容: MIPS processor architecture is a type

删除的内容: of

删除的内容: has

删除的内容: was

删除的内容: WRF-CAMx

删除的内容: The CAMx takes about 15.2 minutes on Loongson 3A4000 CPU and 4.8 minutes on Intel Xeon E5-2697 v4 CPU, when simulating a 2h-case with four parallel processes using MPICH.

39 single-core computing capability of Loongson 3A4000 CPU for the WRF-CAMx  
40 modeling system is about one-third of Intel Xeon E5-2697 v4 CPU and Loongson  
41 3A6000 CPU is slightly lower than Intel Xeon E5-2697 v4 CPU, but the thermal design  
42 power (TDP) of Loongson 3A4000 is 40W, while the Loongson 3A6000 is 38W, only  
43 about one-fourth of Intel Xeon E5-2697 v4, whose TDP is 145W. The results also verify  
44 the feasibility of cross-platform porting and the scientific usability of the ported model.  
45 This study provides a technical foundation for the porting and optimization of  
46 numerical models based on MIPS, LoongArch or other RISC platforms.

删除的内容: 30

删除的内容: one-fifth

删除的内容: which

删除的内容: Thus, Loongson 3A4000 has higher energy efficiency in the application of the WRF-CAMx modeling system.

47

## 48 1 Introduction

49 In the recent years, with the increasing demand for high-performance computing  
50 resources and rapid development in the computer industry, especially supercomputer,  
51 central processing unit (CPU) has undergone significant advancements in logical  
52 structure, operational efficiency, and functional capabilities, making it the core  
53 component of current computer technology development. There are two main types:  
54 one is complex instruction set computer (CISC) CPU (George, 1990; Shi, 2008), mainly  
55 using X86 architecture, representative vendors including Intel, AMD, etc., and widely  
56 used in high-performance computing platforms. The other is reduced instruction set  
57 computer (RISC) CPU (Mallach, 1991; Liu et al., 2022), mainly using ARM, MIPS,  
58 RISC-V and other architectures, representative vendors including Loongson, etc., and  
59 mainly used in high-performance computing platforms, which have high efficiency,  
60 excellent stability and scalability. The Microprocessor without interlocked piped stages  
61 (MIPS) architecture is one of the significant representatives of RISC architecture. MIPS  
62 was originally developed in the early 1980s by Professor Hennessy at Stanford  
63 University and his group (Hennessy et al., 1982). The simplicity of the MIPS instruction  
64 set contributes to its ability to process instructions quickly, thus achieving higher  
65 performance even in low-power conditions. In 1999, MIPS Technology Inc. released  
66 the MIPS32 and MIPS64 architecture standard (MIPS Technology Inc., 2014).  
67 Compared to the CISC CPUs, RISC CPUs demonstrate excellent performance and

74 power efficiency, which have gained popularity among chip manufacturers.

75 The Loongson processor family developed by Loongson Technology is mainly  
76 designed using MIPS architecture and Linux operating system (Hu et al, 2011), which  
77 has rich application tools in Linux open-source projects. The main reason that currently  
78 restricts the development of CPUs that implement non-X86 instruction set architecture  
79 such as MIPS64 is the immature software ecosystem (Hu et al., 2016). Based on the  
80 strategy of open-source software, Loongson platform has gained abundant software  
81 tools, making it possible to further develop scientific computing and numerical models.

82 Air quality model (AQM) systems use mathematical equations and algorithms to  
83 simulate and predict the pollutant concentration in the atmosphere. The current AQMs  
84 have become more complex, incorporating numerous factors such as emissions from  
85 industrial sources, vehicle traffic, and natural sources, as well as meteorological  
86 conditions, including modeling meteorology, emissions, chemical reactions, and  
87 removal processes (Zhang et al., 2012). Regional-scale AQMs have been widely used  
88 to predict air quality in cities, formulate emission reduction strategies, and evaluate the  
89 effectiveness of control policies (Wang et al., 2023), including the Community  
90 Multiscale Air Quality (CMAQ) modelling system (Appel et al., 2017; Appel et al.,  
91 2021), the Comprehensive Air Quality Model with extensions (CAMx; RAMBOLL  
92 ENVIRON Inc., 2014), and the Nested Air Quality Prediction Modeling System (Wang  
93 et al., 2006; Chen et al., 2015). Due to the requirement of meteorological input,  
94 commonly used offline meteorological models such as WRF (Michalakes et al., 2001)  
95 are coupled offline with the regional AQMs to provide meteorological and chemical  
96 forecast as the WRF-AQM modeling system, such the WRF-CMAQ modeling system  
97 (Wu et al., 2014).

98 Both the meteorological and air quality numerical simulation rely heavily on high-  
99 performance computing systems. The WRF-AQM systems can run stably on high-  
100 performance computing platforms based on X86 or X86-compatible instruction set  
101 architecture (ISA) CPUs, which account for the highest percentage among the main  
102 processors of current high performance computing platforms. There are relatively  
103 limited researches on the application of WRF-AQM system on MIPS [and LoongArch](#)

104 CPU platforms at present, this study focuses on the application of WRF-CAMx model  
105 on Loongson CPU platform based on the MIPS [and LoongArch](#) architectures. A  
106 simulation case covering the Beijing-Tianjin-Hebei region was set up to evaluate the  
107 differences and performance between MIPS and X86 platforms. This study validated  
108 the stability of scientific computing on MIPS [and LoongArch](#) CPU platform, and it  
109 offered technical references and evaluation methods for the porting and application of  
110 numerical models on non-X86 platforms.

111 Section 2 provides the model descriptions of the Weather Research and  
112 Forecasting-Comprehensive Air Quality Model with extensions (WRF-CAMx)  
113 modeling system, and the descriptions of MIPS, [LoongArch](#) and benchmark platforms.  
114 The configuration of the air quality numerical simulation system and simulation case  
115 are also presented in Section 2. Section 3 describes porting and optimization of the  
116 WRF-CAMx modelling system on MIPS [and LoongArch](#) CPU platforms. Section 4  
117 analyzes the differences of model results between MIPS CPU platform and the  
118 benchmark platform. Section 5 discusses MIPS [and LoongArch](#) CPUs performance in  
119 scientific computing. The conclusions are presented in Section 6.

120

## 121 **2 Model and Porting Platform Description**

122 The air quality modeling system was constructed using the WRF v4.0 model  
123 developed by National Center for Atmospheric Research (NCAR) (Skamarock et al.,  
124 2019), and the CAMx v6.10 developed by Ramboll Environment (RAMBOLL  
125 ENVIRON Inc., 2014), as shown in Figure 1. And the Loongson 3A4000 CPU platform  
126 was chosen for the porting work in the study. This study introduced the porting of WRF-  
127 CAMx modeling system to MIPS [and LoongArch](#) CPU platforms.

删除的内容:

删除的内容: The remainder is organized as follows.

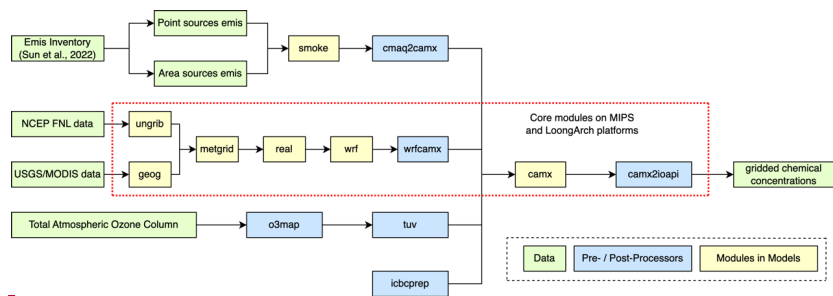
删除的内容: platform

删除的内容: both

删除的内容:

删除的内容: CPU

删除的内容: and benchmark platform



135

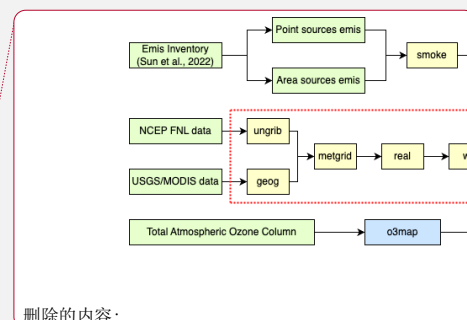
136 **Figure 1.** Framework of WRF-CAMx modeling system. The core modules have been  
 137 ported to MIPS [and LoongArch](#) CPU platforms. The core modules are framed by red  
 138 dashed line in the figure.

139 In Xi'an, China and Milan, [Italy](#), the WRF-CAMx modelling system was [applied](#),  
 140 enabling high-resolution hourly model output of pollutant concentration within specific  
 141 local urban areas (Pepe et al., 2016; Yang et al., 2020). The modeling system is widely  
 142 used to study the spatial-temporal variation of pollutant concentration and source  
 143 apportionment, analyze the contribution of regional transport to pollution and  
 144 investigate the impact of initial conditions and emissions on pollution simulation in key  
 145 regions such as the North China Plain, Sichuan Basin, and Fenwei Plain (Bai et al.,  
 146 2021; Zhen et al., 2023; Zhang et al., 2022; Xiao et al., 2021).

147

## 148 2.1 Description of WRF-CAMx modeling system

149 WRF and CAMx serve as the core components of the modeling system. [WRF is a](#)  
 150 [mesoscale numerical weather prediction system designed for atmospheric research and](#)  
 151 [operational forecasting applications. Distinguished by its high temporal and spatial](#)  
 152 [resolution, WRF is suitable for multi-scale simulations of short-term weather forecast,](#)  
 153 [atmospheric process, and long-term climate, making it an essential tool in the](#)  
 154 [meteorological and atmospheric research communities \(Powers et al., 2017\).](#) In the  
 155 modeling system, WRF provided gridded meteorological field data for air quality  
 156 model CAMx. [The relative humidity, a meteorological variable used in result validation](#)  
 157 [is calculated using the wrf-python package \(Official website: \[https://wrf-\]\(https://wrf-python.readthedocs.io\)](#)  
 158 [python.readthedocs.io, last access: October 2023\).](#) CAMx is an atmospheric pollutant



删除的内容:

删除的内容: '

删除的内容: Europe

删除的内容: developed

删除的内容: WRF is a high-resolution mesoscale model, which can be utilized for various purposes such as weather research and forecasting, physical parameterization scheme research, data assimilation and mesoscale climate simulation.

已移动(插入) [2]

删除的内容: Relative humidity

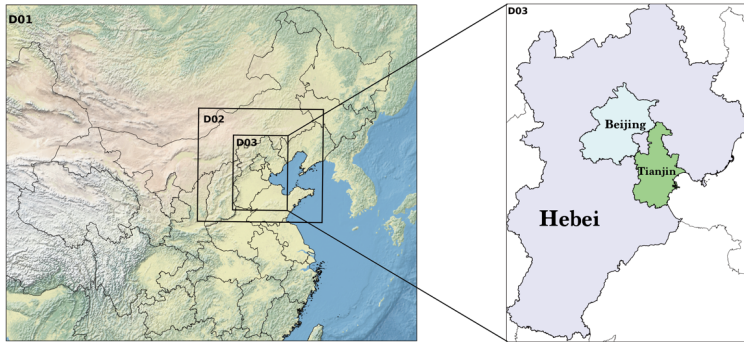
168 calculation model, which can be utilized for simulating and predicting the  
169 concentrations of various air pollutants. The WRF and CAMx models are distinguished  
170 by modularity and parallelism, using MPI in parallel computing, making them efficient  
171 (Skamarock et al., 2019; RAMBOLL ENVIRON Inc., 2014).

172 In the modeling system, the SMOKE model and cmaq2camx program are used to  
173 process emission data and provide model-ready gridded emission data for the CAMx  
174 model. The wrfcamx program converts the WRF results into meteorological input files  
175 which are compatible with CAMx. TUV is a radiation transfer model capable of  
176 producing clean sky photolysis rate input files for the chemical mechanisms in CAMx,  
177 and the o3map program prepares ozone column input files for TUV and CAMx. The  
178 icbcprep program prepares initial and boundary condition files for CAMx with the  
179 profile, and the effects of initial conditions have been studied by Xiao et al. (2021). The  
180 camx2ioapi program converts the CAMx output files into netCDF format following the  
181 Models-3/IO-API convention, and then uses NCL or other softwares to analyses the  
182 model results.

183

### 184 **2.1.1 Model domain setup**

185 The model domain focusing on the Beijing-Tianjin-Hebei region has been set up  
186 in this study. The WRF model has three nested domains with horizontal resolutions of  
187 27km (D1), 9km (D2), and 3km (D3), as shown in Figure 2. The outer domain (D1)  
188 covers most parts of China, and the inner domain (D3) covers Beijing, Tianjin, and  
189 Hebei Province. The model domain is centered at (35°N, 110°E), with two true latitudes  
190 located at 20°N and 50°N. The vertical resolution of WRF is 34 vertical layers. The  
191 CAMx model has only one model domain, which is the innermost grid with a resolution  
192 of 3km (D3), mainly covering the Beijing-Tianjin-Hebei region. The vertical resolution  
193 of CAMx is 14 vertical layers, which is extracted from the WRF output files using the  
194 wrfcamx module, and the lower seven layers of CAMx are same as those in the WRF  
195 model.



196 **Figure 2.** The domains of three-level nested grids in the WRF-CAMx modelling system.  
 197 The respective horizontal resolutions are 27 km × 27 km (D1), 9 km × 9 km (D2), and  
 198 3 km × 3 km (D3).  
 199

200

### 201 2.1.2 Model configuration

202 Starting from 00:00 on November 3, 2020, until 24:00 on November 5, 2020, the  
 203 modelling system simulated the meteorological and air quality for a period of 72 hours,  
 204 represents a moderate-sized real scientific workload, which allows for testing in a short  
 205 time to validate the results and assess computational efficiency on the MIPS and  
 206 LoongArch platforms. For the meteorological model, the global meteorological initial  
 207 and boundary fields for the WRF model are derived from the NCEP Global Final  
 208 Reanalysis Data (FNL), with a spatial resolution of 0.5° x 0.5° and a temporal resolution  
 209 of 6 hours. And the parameterization schemes of the WRF model used in the simulation  
 210 case are shown in Table 1.

211 For the air quality model, the meteorological files are provided by the WRF model  
 212 are used for the chemical transport module in CAMx. The emission inventory used in  
 213 the simulation case was obtained from Sun et al. (2022a). It contains basic emissions  
 214 from Sun et al. (2022b) and fugitive dust emission from bare ground surfaces. The  
 215 SMOKE model (v2.4) is used to process the emission inventory and provide gridded  
 216 emissions for CAMx. The parameterization schemes of the CAMx model used in the  
 217 simulation case are shown in Table 2.

已移动(插入) [1]

删除的内容: , and

删除的内容: validating

删除的内容: of the WRF-CAMx model on the MIPS platform

删除的内容: assessing

223

224 **Table 1.** Parameterization schemes of WRF in research case.

Parameterization process	Scheme
Microphysics	WSM3
Longwave radiation	RRTM
Shortwave radiation	Dudhia
Land surface	Noah
Planetary boundary layer	YSU
Cumulus parameterization	Kain-Fritsch(new Eta)

225

226 **Table 2.** Parameterization schemes of CAMx in research case.

Parameterization process	Scheme
Horizontal Diffusion	PPM
Vertical Diffusion	K-theory
Dry Deposition	Zhang03
Gas-phase chemical mechanism	CB05
Aqueous aerosol chemistry	RADM-AQ
Inorganic gas-aerosol partitioning	ISORROPIA

227

### 228 2.1.3 Statistical indicators for model results

229 To quantify the differences in the model results between the MIPS and benchmark  
 230 platform, three statistical indicators are used to analyze the differences of concentration  
 231 time series: Mean Absolute Error (MAE), Root Mean Square Error (RMSE), and Mean  
 232 Absolute Percentage Error (MAPE). The MAPE quantifies the deviation between  
 233 computational differences and simulated values. The smaller these indicators, the better  
 234 accuracy and stability of scientific computing of the modeling system on the MIPS  
 235 platform. The calculation formulas for these statistical indicators are provided in  
 236 equations (1) to (3).

已移动(插入) [3]

$$237 \quad MAE = \frac{1}{n} \sum_{i=1}^n |MIPS(i) - Base(i)| \quad (1)$$

$$238 \quad RMSE = \left[ \frac{1}{n} \sum_{i=1}^n (MIPS(i) - Base(i))^2 \right]^{\frac{1}{2}} \quad (2)$$

$$239 \quad MAPE = \frac{1}{n} \sum_{i=1}^n \left| \frac{MIPS(i) - Base(i)}{MIPS(i)} \right| \times 100\% \quad (3)$$

240 In the equations,  $n$  represents the number of grids in the domain.  $MIPS(i)$  represents the  
 241 simulated value of a certain grid on the MIPS platform, and  $Base(i)$  represents the



242 baseline value of a certain grid on the benchmark platform.

243

## 244 2.2 MIPS and LoongArch CPU platforms description

245 Loongson CPU platform was chosen for the porting work in the study. Currently,  
246 the Loongson processor family has three generations of CPU products, evolving from  
247 single-core to multi-cores architectures and from experimental prototypes to mass-  
248 produced industrial products (Hu et al., 2011). The Loongson-2 processor is a 64-bit  
249 general-purpose RISC processor series which is compatible with MIPS instruction set.  
250 It can be used in personal computers, mobile terminals, and various embedded  
251 applications, running many operating systems such as Linux and Android smoothly  
252 (Zhi et al., 2012). Wu et al. (2019) reports the application of the mesoscale model on  
253 Loongson 2F CPU platform. The Loongson-3 processor features a scalable multi-core  
254 architecture, targeting high-throughput data centers, high-performance scientific  
255 computing, and other applications, with the significant advantage of achieving a high  
256 peak performance-to-power ratio and striking a well-balanced trade-off between  
257 performance and power consumption (Hu et al., 2009).

258 The Loongson 3A series are multi-core processors designed for high-performance  
259 computers, featuring with high bandwidth, and low power consumption. The efficient  
260 design solution and the advantage of high energy efficiency ratio make servers based  
261 on Loongson CPUs highly competitive in performance, power consumption, and cost-  
262 effectiveness (Li et al., 2014; Wang et al., 2014). In this study, the Loongson platform  
263 uses the Debian Linux operating system, commercially known as Tongxin UOS  
264 (<https://www.uniontech.com>, last access: January, 2024), and the Loongson 3A4000  
265 processor, which is the first quad-core processor based on GS464v 64-bit  
266 microarchitecture in Loongson 3 Processor Family. The main technical parameters of  
267 Loongson 3A4000 CPU are shown in Table 3. Compared to previously released CPUs,  
268 the processor improves frequency and performance by optimizing on-chip interconnect  
269 and memory access path, integrating 64-bit DDR4 memory controller and on-chip  
270 security mechanism. The Loongson 3A6000 CPU platform uses Loongnix, the open-  
271 source community edition operating system released by Loongson

删除的内容: ↵

A lot of porting and optimization research work has been conducted to ensure the proper functioning of the high-performance mathematical library on Loongson platforms, resulting in improved computing performance, such as FFT (Fast Fourier Transform) (Guo et al., 2012; Li et al., 2011; Zhao et al., 2012). The porting and optimization efforts conducted on the multi-core Loongson processors have successfully demonstrated the stability and efficiency in the numerical computing applications. These results provide valuable technical references and rationality validation for the numerical model application on Loongson platform.

删除的内容: <https://www>

**带格式的:** 默认段落字体, 字体: (默认) +西文正文 (DengXian), 五号

删除的内容: October 2023

**带格式的:** 默认段落字体, 字体: (默认) +西文正文 (DengXian), 五号

286 (<https://www.loongson.cn/system/loongnix>, last access: January, 2024), and the latest  
 287 released Loongson 3A46000 processor, which is a quad-core processor based on LA664  
 288 microarchitecture. The main technical parameters of Loongson 3A6000 CPU are shown  
 289 in Table 3. The processor supports the LoongArch™ instruction set and hyper-threading,  
 290 and the performance has significantly improved compared to the previously released  
 291 processors (Hu et al., 2022).

删除的内容: <https://www>  
 带格式的: 默认段落字体, 字体: (默认) +西文正文 (DengXian), 五号  
 带格式的: 默认段落字体, 字体: (默认) +西文正文 (DengXian), 五号

292

293 **Table 3.** Main Parameters of [Loongson 3A4000 CPU](#) and [Loongson 3A6000 CPU](#)\*

<a href="#">Main Parameters</a>	<a href="#">Loongson 3A4000 CPU</a>	<a href="#">Loongson 3A6000 CPU</a>
<a href="#">Main Frequency</a>	<a href="#">1.8GHz–2.0GHz</a>	<a href="#">2.0GHz–2.5GHz</a>
<a href="#">Peak Computing Speed</a>	<a href="#">128Gflops@2.0GHz</a>	<a href="#">240Gflops</a>
<a href="#">Transistor Technology</a>	<a href="#">28nm</a>	<a href="#">12nm</a>
<a href="#">Number of Cores</a>	<a href="#">4</a>	<a href="#">4(Physical) 8(Logical)</a>
<a href="#">Processor Cores</a>	<a href="#">MIPS64 compatible Support 128/256-bit vector instructions</a>	<a href="#">support LoongArch™ Support 128/256-bit vector instructions</a>
<a href="#">High-speed I/O</a>	<a href="#">2 x 16-bit HyperTransport 3.0 control</a>	<a href="#">1 x HyperTransport 3.0 control</a>
<a href="#">Typical Power Consumption</a>	<a href="#">&lt;30W@1.5GHz &lt;40W@1.8GHz &lt;50W@2.0GHz</a>	<a href="#">38W@2.5GHz</a>

删除的内容:  
 删除的内容: [Loogson 3A4000 CPU](#)

294 \*source: <https://www.loongson.cn>, last access: [January, 2024](#).

删除的内容: [Loongson 3A4000 CPU Main Parameters](#) ... [1]  
 删除的内容: October 2023

295

296 **2.3 Benchmark platform description**

297 This study uses an X86 CPU platform as benchmark platform compared to the  
 298 MIPS [and LoongArch CPU platforms](#). The benchmark platform is powered by Intel  
 299 Xeon E5-2697 v4 CPU, with strong floating-point performance and many technical  
 300 features such as Intel Turbo Boost Technology (Intel Inc., 2023). The Intel Xeon E5-  
 301 2697 v4 CPU has 18 cores, with 2.3GHz base frequency and 3.6GHz maximum Turbo  
 302 Boost frequency, 45 MB Intel Smart Cache and 145W design power consumption. The  
 303 operating system is CentOS Linux 7.4.1708. The main information for [all platforms](#) is  
 304 shown in Table 4.

删除的内容: CPU platform

删除的内容: both

305

313 **Table 4.** The comparison of main configuration between MIPS, [LoongArch](#) and X86  
 314 platforms.

	<u>MIPS Platform</u>	<u>LoongArch Platform</u>	<u>X86 platform</u>
<u>CPU</u>	<a href="#">Loongson 3A4000</a>	<a href="#">Loongson 3A6000</a>	<a href="#">Intel Xeon E5-2697 v4</a>
<u>Number of CPUs</u>	<a href="#">1</a>	<a href="#">1</a>	<a href="#">1</a>
<u>Number of CPU cores</u>	<a href="#">4</a>	<a href="#">8</a>	<a href="#">18</a>
<u>CPU Frequency</u>	<a href="#">1.8GHz</a>	<a href="#">2.0Ghz</a>	<a href="#">2.3GHz</a>
<u>CPU instruction set</u>	<a href="#">MIPS64</a>	<a href="#">LoongArch™</a>	<a href="#">X86_64</a>
<u>Operating system</u>	<a href="#">Tongxin UOS</a>	<a href="#">Loongnix</a>	<a href="#">CentOS Linux 7.4.1708</a>
<u>Operating system kernel (Linux version)</u>	<a href="#">4.19.0-loongson-3- desktop</a>	<a href="#">4.19.0-19- loongson-3</a>	<a href="#">3.10.0- 957.1.3.el7.x86_64</a>

带格式的: 居中

带格式的: 居中

带格式的: 居中

带格式的: 居中

带格式的: 居中

带格式的: 居中

带格式的: 居中

带格式的: 居中

315  
316

删除的内容: [MIPS Platform](#) ... [2]

317 **2.4 The difference between MIPS, [LoongArch](#) and X86 platforms**

318 In this study, the numerical model's source code is written in Fortran, and  
 319 commonly used compilers for X86 architecture include Intel Compiler, PGI and GNU  
 320 Compiler. The compiler for MIPS platform is built using GCC 8.3 MIPS GNU/Linux  
 321 cross-toolchain based on the open-source GNU Project, called MIPS GNU, and the  
 322 latest version is 8.3. [And the compiler for LoongArch platform is built using GCC 8.3](#)  
 323 [LoongArch GNU/Linux cross-toolchain based on the open-source GNU Project, called](#)  
 324 [LoongArch GNU, and the latest version is 8.3.](#) The compiler for the benchmark  
 325 platform is set to X86 GNU, and the version is also 8.3. Table 5 shows the differences  
 326 between [all platforms'](#) GNU compilers in terms of applicable platforms. Compared to  
 327 X86 GNU, the default compilation options of MIPS GNU compiler not only specify  
 328 the platform architecture but also include additional instruction sets, such as atomic  
 329 operation instruction set LLSC, shared library instruction set PLT, etc., which can  
 330 optimize target programs compiled by GNU for MIPS architecture and improve

删除的内容: the two

删除的内容: '

335 computational efficiency. [And the default compilation options of LoongArch GNU](#)  
 336 [compiler not only specify the platform architecture but also include target](#)  
 337 [microarchitecture tuning option, which can also optimize target programs compiled by](#)  
 338 [GNU for LoongArch architecture.](#)

339 **Table 5.** Comparison of GNU compiler between MIPS, [LoongArch](#) and X86 CPU  
 340 platforms.

<a href="#">Artitecture</a>	<a href="#">MIPS64</a>	<a href="#">LoongArch</a>	<a href="#">x86_64</a>
<a href="#">Compiler</a>	MIPS GNU Fortran	<a href="#">LoongArch GNU Fortran</a>	X86 GNU Fortran
<a href="#">Version</a>	<a href="#">8.3</a>	<a href="#">8.3</a>	<a href="#">8.3</a>
<a href="#">Target</a>	<a href="#">mips64el-linux-gnuabi64</a>	<a href="#">loongarch64-linux-gnu</a>	<a href="#">x86_64-redhat-linux</a>
<a href="#">Options (Architecture)</a>	<a href="#">-march=mips64r2 -mabi=64</a>	<a href="#">-march=loongarch64 -mabi=lp64d</a>	<a href="#">-march=x86-64 -mtune=generic</a>
<a href="#">Options (Instruction set)</a>	<a href="#">-mllsc -mplt -mmadd4</a>	<a href="#">-mtune=loongarch64</a>	<a href="#">/</a>
<a href="#">FLAGS(WRF)</a>	<a href="#">-fconvert=big-endian -frecord-marker=4 -ffree-line-length-none -O2 -ftree-vectorize -funroll-loops</a>		
<a href="#">FLAGS(CAMx)</a>	<a href="#">-fconvert=big-endian -frecord-marker=4 -ffixed-line-length-none -fno-align-commons -O2</a>		

341 The WRF-CAMx modeling system depends on several scientific computing  
 342 libraries. Firstly, the general data format libraries netCDF and HDF5 are required to  
 343 store the large-scale gridded data for the modeling system. NetCDF is a self-describing  
 344 data format developed by NCAR/Unidata, primarily used for storing multidimensional  
 345 array data in fields like meteorology and earth sciences (UCAR/Unidata, 2021). HDF5  
 346 is a data format developed by HDF GROUP that supports complex data structures with  
 347 multiple data types and multi-dimensional datasets (The HDF Group, 2019). In this  
 348 study, netCDF-C (v4.8.1), netCDF-Fortran (v4.5.3), HDF5 (v1.12.1) and IOAPI (v3.1)  
 349 were successfully installed on MIPS [and LoongArch](#) platforms by building from their  
 350 sources, which are obtained from the official website.

351 The MPICH library is required to support parallel computing in the modeling  
 352 system. In order to fully utilize computing resources, the method of MPI message  
 353 communication is used in WRF and CAMx model (Wu et al., 2012). MPICH is an  
 354 open-source, portable parallel computing library for implementing the MPI standard

删除的内容: **Artitecture** ... [3]

356 (Amer et al., 2021). It supports inter-process communication and data exchange in the  
357 parallel computing environment. Similarly, this study successfully installed MPICH  
358 (v3.4) on MIPS [and LoongArch](#) platforms by building from its source. During the  
359 compilation and installation of the mentioned libraries above, the configure tool was  
360 used to check the basic information of the platform's CPU and compiler, and prepare  
361 for compatibility with platform before compilation, the GNU compiler is used to  
362 compile the source code of libraries, and the cmake tool is used to install the libraries.  
363 Additionally, the same runtime environment as MIPS platform was also built on the  
364 benchmark platform.

365

### 366 **3 Porting the WRF-CAMx modelling system on MIPS [and LoongArch](#)** 367 **CPU platforms**

368 The simulation result is influenced by several factors including processor  
369 architecture, operating system, compiler, parallel environment, and scientific  
370 computing libraries. In order to ensure stability and accuracy of numerical simulation,  
371 the models should be adapted to the new runtime environment when porting across  
372 platforms. Additionally, various operating systems have different tools, software and  
373 libraries, which may impact the results of numerical simulations.

374 In this study, the runtime environment for WRF-CAMx modeling system was built  
375 on MIPS [and LoongArch](#) platforms. The configuration files for making the models were  
376 modified to fit the compilers of the Linux system on MIPS [and LoongArch](#) platforms.  
377 In order to verify the stability of scientific computing on MIPS [and LoongArch](#)  
378 platforms, a control experiment was set up on the benchmark platform, minimizing the  
379 impact of other factors on simulation results of both platforms.

380 The WRF v4.0 and CAMx v6.10 were successfully deployed on MIPS [and](#)  
381 [LoongArch](#) platforms through source code compilation and installation. In the WRF  
382 model, the default options for GNU compiler which are suitable for MIPS [and](#)  
383 [LoongArch](#) architecture CPUs are not provided in the configure file of the source code  
384 package, and it is necessary to manually add information about the CPU architecture,

删除的内容: UOS

386 GNU compiler, and compilation flags on MIPS [and LoongArch](#) platforms. Table 5  
387 provides the detailed information added in the configure file, mainly about MIPS [and](#)  
388 [LoongArch](#) GNU Fortran. When compiling Fortran programs on MIPS [and LoongArch](#)  
389 platforms, the MIPS [and LoongArch](#) GNU Fortran and necessary compilation flags  
390 must be specified. These flags include common Fortran file format flags such as -  
391 fconvert=big-endian and -frecord-marker=4, as well as optimization flags such as -O2  
392 -ftree-vectorize -funroll-loops. By specifying the appropriate compiler and flags for  
393 MIPS [an LoongArch](#) architectures, the configure tool will provide necessary settings to  
394 compile WRF. Correspondingly, when compiling WRF on the benchmark platform, the  
395 compilation flags are strictly consistent with those of MIPS [and LoongArch](#) CPU  
396 platforms, which ensures that differences in simulation results of two platforms are  
397 primarily attributed to the underlying hardware architecture rather than changes in  
398 compilation settings.

399 In the CAMx model, the makefile provides information about parallelism and  
400 compilers. Similarly, information about the CPU architecture, GNU compiler, and  
401 compilation flags on MIPS [and LoongArch](#) platforms also needs to be added in the  
402 makefile. For the detailed information added in the makefile, please refer to Table 5. So  
403 far, the WRF-CAMx model has been successfully compiled and installed on the MIPS  
404 [and LoongArch](#) platforms after modifications of the configuration files mentioned  
405 above.

406

## 407 **4 The differences of model results on the two platforms**

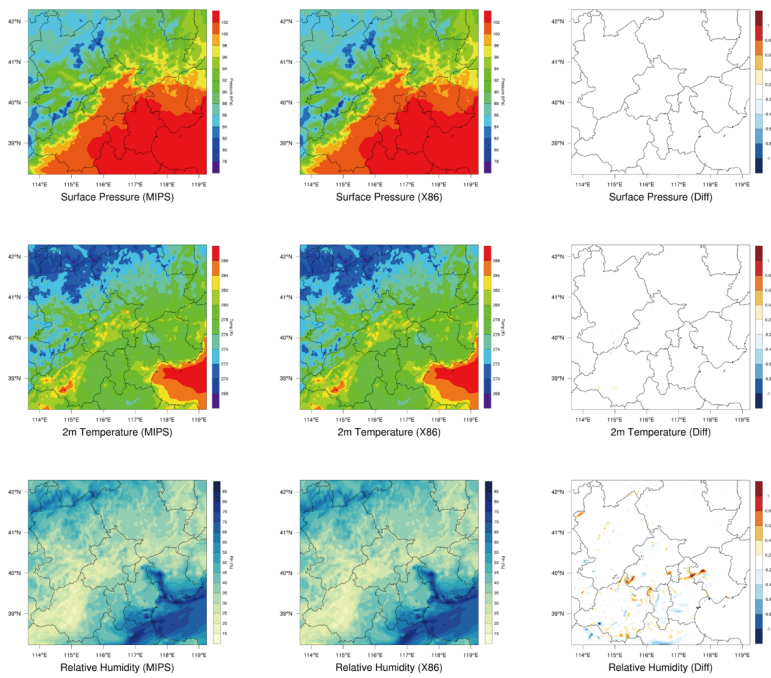
### 408 **4.1 Validation of the spatial distribution**

409 A [72h](#) simulation case has been designed to test the stability and availability of the  
410 WRF-CAMx modeling system on the MIPS CPU platform in Beijing. By analyzing the  
411 differences in simulation results and computing time, the accuracy and performance of  
412 the modeling system on MIPS platform were evaluated, which further verifies the  
413 feasibility and stability of the modeling system after porting to the MIPS platform.

414 Common meteorological variables, including 2-meter temperature, land surface

已上移 [1]: Starting from 00:00 on November 3, 2020, until 24:00 on November 5, 2020, the modelling system simulated the meteorological and air quality for a period of 72 hours, represents a moderate-sized real scientific workload, which allows for testing in a short time, and validating the results of the WRF-CAMx model on the MIPS platform and assessing computational efficiency.

422 pressure, and relative humidity were selected to verify the WRF model results. Figure  
 423 3 shows the spatial distribution of the four meteorological variables after 72 hours  
 424 simulation on different platforms, as well as the absolute errors (AEs). The  
 425 meteorological variables from the modeling system on the different platforms exhibit a  
 426 generally consistent spatial distribution in the Beijing-Tianjin-Hebei regions shown in  
 427 Figure 3.

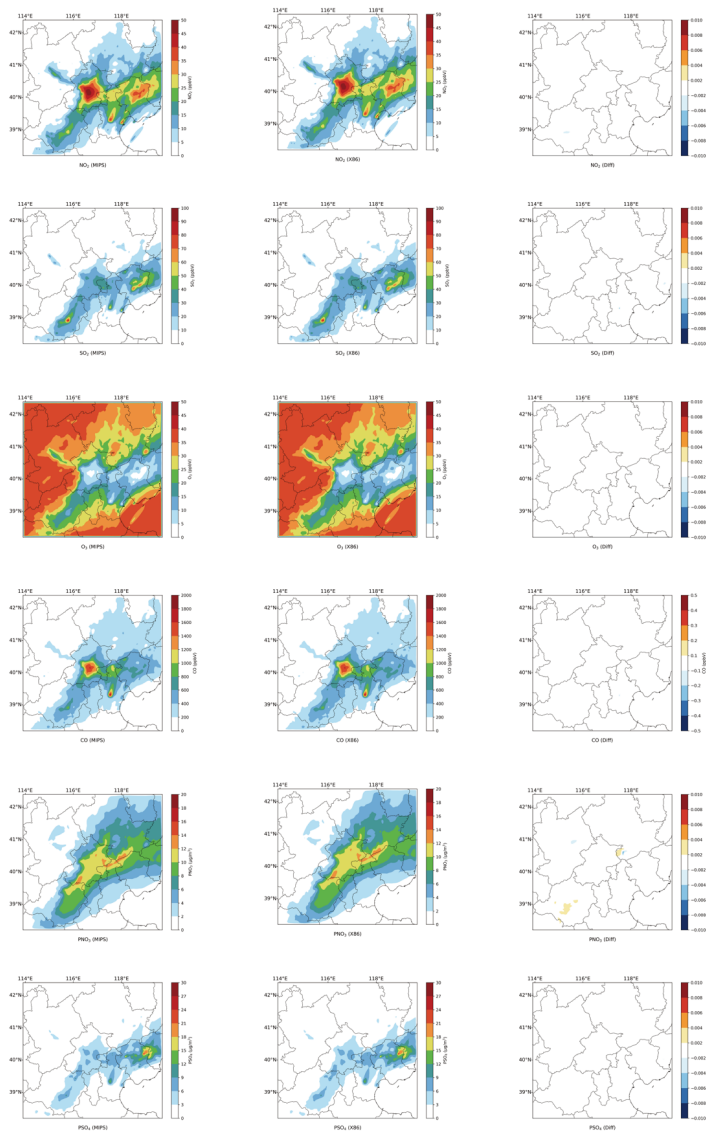


428 **Figure 3.** Spatial distribution of 2m temperature, surface pressure, relative humidity  
 429 from WRF. Left column, MIPS platform. Middle, the X86 platform. Right, the  
 430 differences between the MIPS and benchmark(X86) platform.  
 431

432  
 433 Similarly, the NO<sub>2</sub>, SO<sub>2</sub>, O<sub>3</sub>, CO, PNO<sub>3</sub> and PSO<sub>4</sub> were selected to verify the  
 434 CAMx model results on the MIPS platform. Figure 4 shows the spatial distribution of  
 435 the six species, as well as the absolute errors (AEs) between the two platforms after 72  
 436 hours simulation. Simulating the 72h-case with four parallel processes using MPICH,

已上移 [2]: Relative humidity is calculated using the wrf-python package (Official website: <https://wrf-python.readthedocs.io>, last access: October 2023).

440 CAMx takes about 9h on Loongson 3A4000 CPU and 2.6h on Intel Xeon E5-2697 v4  
 441 CPU. As shown in Figure 4, the spatial distribution of air pollution concentrations from  
 442 the different platforms is essentially consistent, appearing very similar visually.

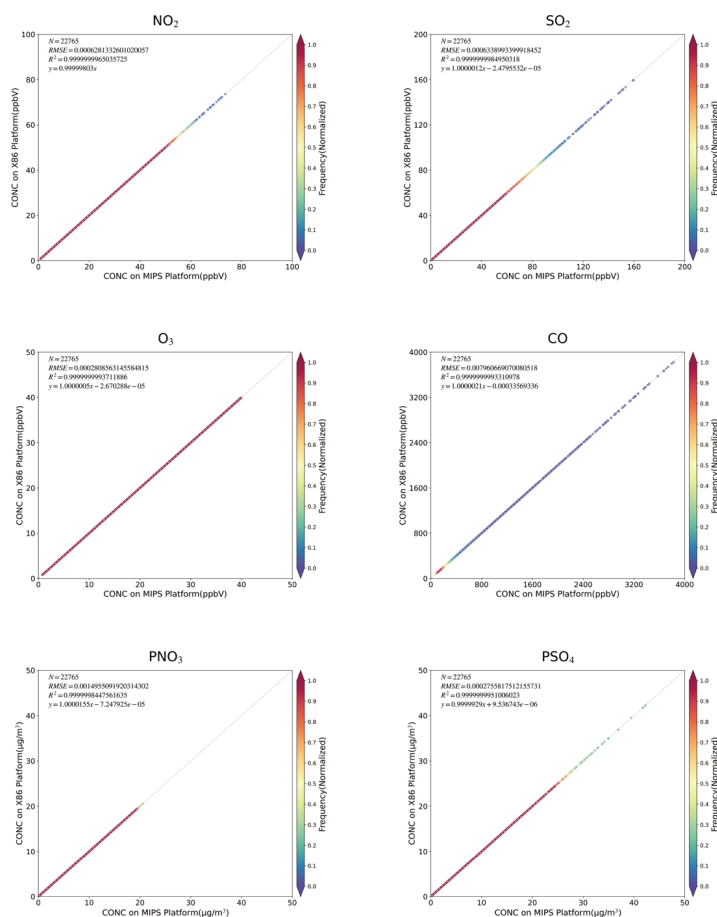


443  
 444 **Figure 4.** Spatial distribution of NO<sub>2</sub>, SO<sub>2</sub>, O<sub>3</sub>, CO, PNO<sub>3</sub> and PSO<sub>4</sub> from CAMx on



445 MIPS and benchmark platform. Left column, MIPS platform. Middle, the X86 platform.  
446 Right, the differences between the MIPS and benchmark(X86) platform.

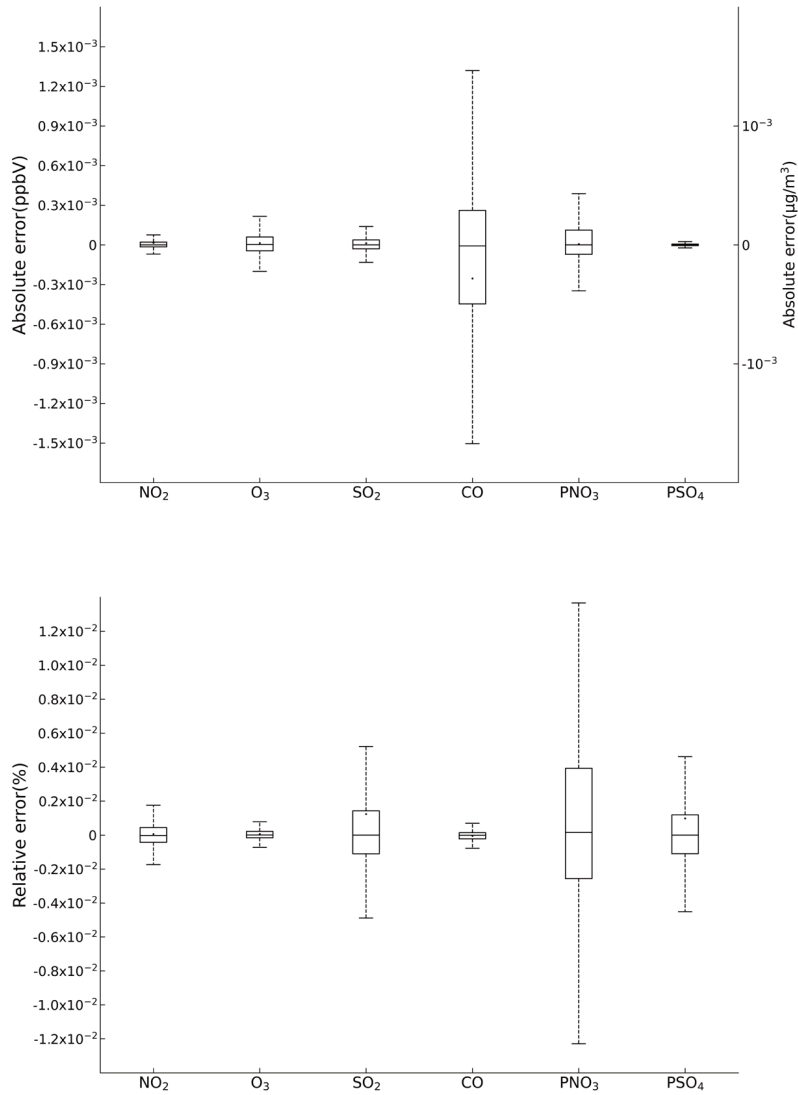
447 As shown in Figure 5, the scatter plots between the two platform, it can be seen  
448 that for the total of 22,765 grids within the 145x157 simulation domain, the root mean  
449 square errors (RMSEs) of the six species between the MIPS platform and benchmark  
450 platform are close to 0.001, which is essentially 0. The linear regression model was  
451 used to fit the scatters, and the regression slopes for each species are nearly 1, with  
452 intercepts close to 0, and the R2 values used for the goodness of fit are nearly 1. The  
453 fitted lines closely coincide with the “y=x” line, indicating that the differences between  
454 the MIPS and X86 platform for each species are minimal to negligible.



455  
 456 **Figure 5.** Scatter of grid concentrations for NO<sub>2</sub>, SO<sub>2</sub>, O<sub>3</sub>, CO, PNO<sub>3</sub> and PSO<sub>4</sub> from  
 457 CAMx on the MIPS and benchmark platform. The density of scatters is represented by  
 458 the colors.

459 Figure 6 is the boxplots which show the absolute errors (AE) and relative errors  
 460 (RE) of the six species between MIPS and benchmark platform. According to Figure 6,  
 461 the absolute errors of the six species are generally in the range of  $\pm 10^{-3}$  ppbv (parts per  
 462 billion by volume; the unit of NO<sub>2</sub>, SO<sub>2</sub>, O<sub>3</sub> and CO concentration) or  $\mu\text{g m}^{-3}$  (the unit  
 463 of particle composition PNO<sub>3</sub> and PSO<sub>4</sub>), and the relative errors are generally in the  
 464 range of  $\pm 0.01\%$ . Specially for CO, it exhibits more pronounced AEs compared to other

465 species. In some grid boxes, the AEs between MIPS and benchmark platform exceed  
466 the range of  $\pm 10^{-3}$  ppbv, but they remain in the range of  $\pm 10^{-2}$  ppbv. In summary, there  
467 are some errors between the results of the modeling system on the MIPS and benchmark  
468 platform during the porting process. However, these errors are relatively minor  
469 compared to the numerical values. The reasons are attributed to the differences in the  
470 CPU architecture and compiler characteristics between the two platforms, such as data  
471 operations and precision running on different CPUs, which are primarily responsible  
472 for the observed errors.



473

474 **Figure 6.** The absolute errors and relative errors for NO<sub>2</sub>, SO<sub>2</sub>, O<sub>3</sub>, CO, PNO<sub>3</sub> and PSO<sub>4</sub>  
 475 concentration in all grids between the MIPS and benchmark platform.

476 Additionally, random grids in the domain were selected to assess the precision of  
 477 simulation results in localized regions. The positions of these grids were determined

478 based on 32 observation stations in Beijing, and the nearest grid was determined using  
479 the Euclidean Shortest Distance in the domain. The station map is presented in Figure  
480 S1 in the Supplement. The Taylor diagram is used to assess the precision of  
481 concentrations for six species near the observation stations, and the scatters  
482 representing the six species at 32 stations are highly overlapping. Statistical parameters  
483 used in the Taylor diagram, such as the correlation coefficient (R) approaching 1,  
484 normalized standard deviation (NSD) and normalized root mean square error (NRMSE)  
485 approaching 0, indicate high precision of the simulation results at specific stations on  
486 the MIPS platform.

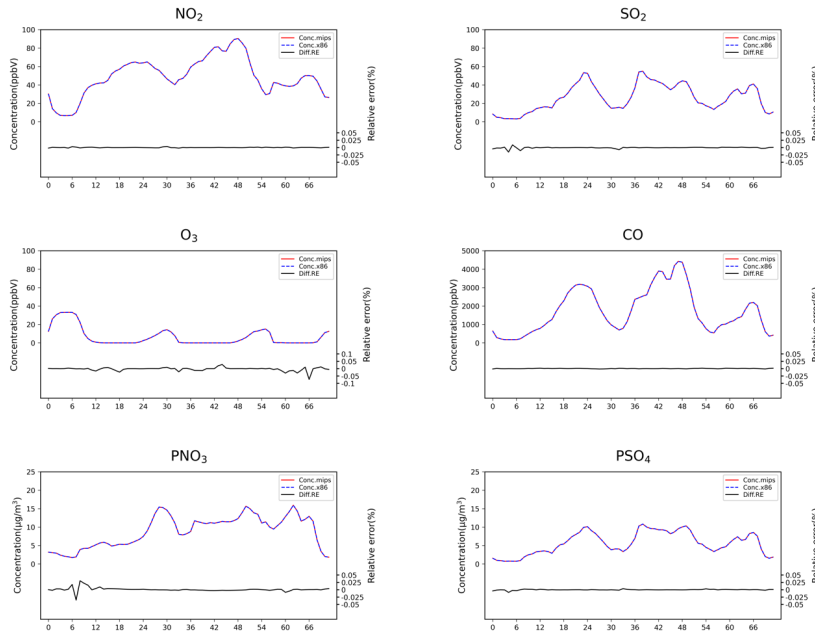
487

#### 488 **4.2 Validation of the temporal distribution from the two platform**

489 The time series of computational differences also be evaluated in this study.  
490 Random grid in the domain was selected to examine the hourly concentrations of the  
491 six species. Taking the example of the Beijing Olympic Center station (116.40°E,  
492 39.99°N) from the National Standard Air Quality (NSAQ) stations, the time series of  
493 hourly concentrations in the grid of the Beijing Olympic Center station and relative  
494 errors between the MIPS and benchmark platform over the 72-hour period were shown  
495 in Figure 7. As shown in Figure 7, it can be seen that the time series of the air pollutant  
496 concentrations were highly consistent between the two platforms. In the 72-hour period,  
497 the relative errors for NO<sub>2</sub>, SO<sub>2</sub>, CO and PSO<sub>4</sub> remain in ±0.025%. For PNO<sub>3</sub>, the  
498 relative errors remain in ±0.05%, and for O<sub>3</sub>, they remain in ±0.1%. This indicates that  
499 the errors caused by different architectures are within a reasonable range.

删除的内容:

删除的内容:



502  
 503 **Figure 7.** Time-series of NO<sub>2</sub>, SO<sub>2</sub>, O<sub>3</sub>, CO, PNO<sub>3</sub> and PSO<sub>4</sub> concentrations and its  
 504 relative errors (RE) at the Beijing Olympic Sports Center site between the MIPS and  
 505 X86 platform. The red solid line and the blue dashed line, the CAMx model results on  
 506 MIPS platform and X86 platform. The black solid line shows the relative errors (RE)  
 507 between the MIPS and X86 platform.

508  
 509 Figure 8 shows the time series of the concentration and their statistical indicators,  
 510 MAE, RMSE, and MAPE during the 72-hour simulation. As show in the figure, for  
 511 NO<sub>2</sub>, SO<sub>2</sub>, O<sub>3</sub>, and PSO<sub>4</sub>, the MAEs are all below 10<sup>-3</sup> ppbv (µg m<sup>-3</sup>), and the RMSEs  
 512 are all below 10<sup>-3</sup>. The MAEs for CO and PNO<sub>3</sub> are below 10<sup>-2</sup> ppbv (µg m<sup>-3</sup>), and the  
 513 RMSEs for PNO<sub>3</sub> are below 10<sup>-2</sup>, while the RMSEs for CO are below 10<sup>-1</sup>. This is  
 514 because that PNO<sub>3</sub> and CO have relatively higher background concentrations compared  
 515 to the other species. The MAPE of PNO<sub>3</sub> concentration mainly ranging in 0-0.5%, while  
 516 the MAPE of CO concentration has the lowest values below 0.001%, and the other  
 517 species are in the range of 0-0.01%. Overall, the above time-series analysis verifies the  
 518 accuracy and stability of the modeling system on the MIPS platform.

已上移 [3]: To quantify the differences in the model results between the MIPS and benchmark platform, three statistical indicators are used to analyze the differences of concentration time series: Mean Absolute Error (MAE), Root Mean Square Error (RMSE), and Mean Absolute Percentage Error (MAPE). The MAPE quantifies the deviation between computational differences and simulated values. The smaller these indicators, the better accuracy and stability of scientific computing of the modeling system on the MIPS platform. The calculation formulas for these statistical indicators are provided in equations (1) to (3).<sup>4</sup>

$$MAE = \frac{1}{n} \sum_{i=1}^n |MIPS(i) - Base(i)| \quad (1)^{4}$$

$$RMSE = \left[ \frac{1}{n} \sum_{i=1}^n (MIPS(i) - Base(i))^2 \right]^{\frac{1}{2}} \quad (2)^{4}$$

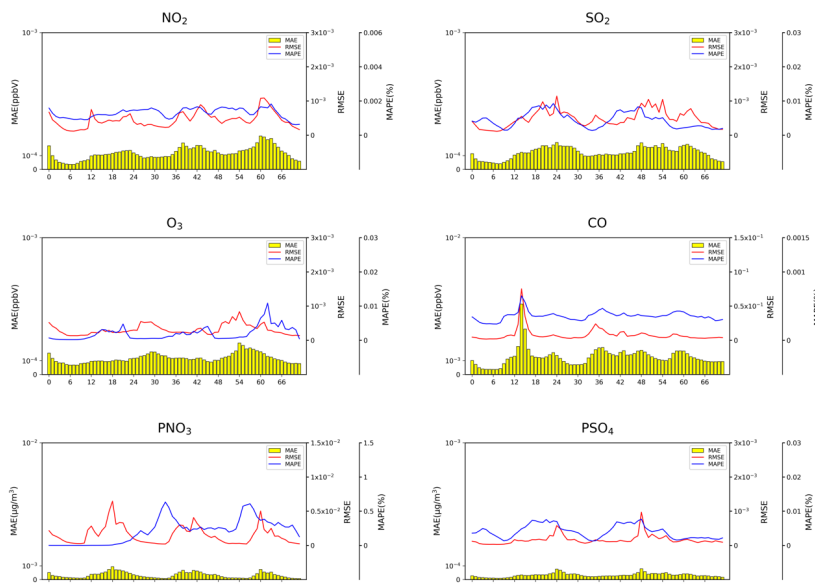
$$MAPE = \frac{1}{n} \sum_{i=1}^n \left| \frac{MIPS(i) - Base(i)}{MIPS(i)} \right| \times 100\% \quad (3)^{4}$$

In the equations,  $n$  represents the number of grids in the domain.  $MIPS(i)$  represents the simulated value of a certain grid on the MIPS platform, and  $Base(i)$  represents the baseline value of a certain grid on the benchmark platform.<sup>4</sup>

删除的内容:  $MAE = \frac{1}{n} \sum_{i=1}^n |MIPS(i) - Base(i)|$

删除的内容:  $RMSE = \left[ \frac{1}{n} \sum_{i=1}^n (MIPS(i) - Base(i))^2 \right]^{\frac{1}{2}}$

删除的内容:  $MAPE = \frac{1}{n} \sum_{i=1}^n \left| \frac{MIPS(i) - Base(i)}{MIPS(i)} \right| \times 100\%$



543

544 **Figure 8.** Time series of MAEs, RMSEs and MAPEs for NO<sub>2</sub>, SO<sub>2</sub>, O<sub>3</sub>, CO, PNO<sub>3</sub> and  
 545 PSO<sub>4</sub> concentration in the 72h simulation. The yellow bar, the MAE. The red lines,  
 546 RMSE, the blue lines, MAPE.

547

548 In this study, the evaluation method proposed by Wang et al. (2021) was also used  
 549 to assess the scientific applicability of the model results on the MIPS platform. The  
 550 [Root Mean Square Errors \(RMSEs\)](#) for NO<sub>2</sub>, SO<sub>2</sub>, O<sub>3</sub>, CO, PNO<sub>3</sub> and PSO<sub>4</sub>  
 551 concentration between the MIPS and benchmark platform were computed, along with  
 552 the standard deviations (*stds*) used to describe the spatial variation of species, and the  
 553 ratio of RMSE to *std*, as shown in Table 6. The differences of the four species between  
 554 the two platforms are negligible compared to their own spatial variations. Therefore,  
 555 the results on the MIPS platform meet the accuracy requirements for research purpose.

556

557 **Table 6.** RMSE, *std*, RMSE/*std* for NO<sub>2</sub>, SO<sub>2</sub>, O<sub>3</sub>, CO, PNO<sub>3</sub> and PSO<sub>4</sub>.

	Differences in results	Spatial variation	RMSE/ <i>std</i>
	RMSE	<i>std</i>	
NO <sub>2</sub>	$6.3 \times 10^{-7}$	0.01	$5.9 \times 10^{-5}$

<b>O<sub>3</sub></b>	$2.8 \times 10^{-7}$	0.01	$2.5 \times 10^{-5}$
<b>SO<sub>2</sub></b>	$6.3 \times 10^{-7}$	0.02	$3.9 \times 10^{-5}$
<b>CO</b>	$7.9 \times 10^{-6}$	0.30	$2.6 \times 10^{-5}$
<b>PNO<sub>3</sub></b>	$1.5 \times 10^{-3}$	3.8	$3.9 \times 10^{-4}$
<b>PSO<sub>4</sub></b>	$2.7 \times 10^{-4}$	3.9	$6.9 \times 10^{-5}$

558

559 In fact, the differences in model results cannot be completely eliminated, primarily  
 560 due to the varying CPU architectures and compilers. In the practical applications,  
 561 compared with the errors arising from the inherent uncertainties of the modeling system  
 562 and the input data, the differences of model results between different platforms can even  
 563 be considered negligible. The comprehensive analysis demonstrates that the results of  
 564 the WRF-CAMx modeling system on the MIPS CPU platform are reasonable.

565

## 566 **5 The evaluation about computational performance**

567 Scientific computing involves a significant amount of floating-point operations,  
 568 and the floating-point computational capability is a crucial indicator for CPU  
 569 performance. In this study, the simulation case was configured to conduct parallel  
 570 computing tests on the MIPS, [LoongArch](#) and benchmark platform. These tests  
 571 included assessing the CPU's single-core performance with the non-parallel model and  
 572 the platform's parallel performance with the parallel model using multiple processes.  
 573 The time of CAMx model running simulation case for [24](#) hours in the modeling system  
 574 are shown in Figure 9. From the figure, it can be observed that under single-core  
 575 conditions, the computing capability of the MIPS platform for CAMx is approximately  
 576 one-third of the X86 benchmark platform, [and the LoongArch platform is slightly lower](#)  
 577 [than the X86 benchmark platform.](#)

578 It's worth noting that the simulation time of the CAMx model for running with two  
 579 processes in parallel and running in non-parallel remains approximately consistent.  
 580 This is because the MPI used in CAMx is designed using a "master/slave" parallel  
 581 processing approach, and a process is allocated for input/output and message  
 582 communication during the runtime (Cao K et al., 2023). This process doesn't perform  
 583 any simulation in the model. Therefore, the time required for parallelism of two

删除的内容: 2



585 processes is comparable to the non-parallelism, and in some cases, it might even be  
586 slightly longer due to the overhead of MPI communication. Compared to non-parallel,  
587 the speedup of the MIPS platform with four-process parallelism using MPICH3 is  
588 approximately 2.8, while using OpenMP is about 2.9. ~~and the speedup of the~~  
589 ~~LoongArch platform with four-process parallelism using MPICH3 is approximately 2.8,~~  
590 ~~while using OpenMP is about 2.9.~~ For the X86 benchmark platform, running with four  
591 processes in parallel using MPICH3 has a speedup of approximately 2.7.

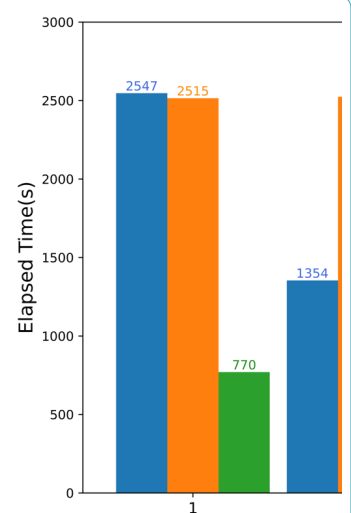
592 Additionally, the performance of the MIPS platform significantly decreases when  
593 the number of parallel processes exceeds 4. This is because the modeling system  
594 involves compute-intensive tasks. The Loongson 3A4000 CPU has four cores, and  
595 when the number of processes called by MPI matches the number of CPU cores, the  
596 CPU utilization can approach 100%. Further increasing the number of processes, the  
597 cores will compete for CPU resources, resulting in additional overhead and reduced  
598 computational efficiency. ~~As for LoongArch platform, the performance slightly~~  
599 ~~decreases when the number of parallel processes exceeds 4. The Loongson 3A6000~~  
600 ~~CPU has four physical cores and eight logical cores, and when the number of processes~~  
601 ~~called by MPI matches the number of physical cores, the computational load is evenly~~  
602 ~~distributed across each core. Although the Loongson 3A6000 supports hyper-threading,~~  
603 ~~further increasing the number of processes, CPU starts to schedule logical cores to~~  
604 ~~allocate computational load. Thread scheduling will result in additional overhead and~~  
605 ~~reduced computational efficiency. This explains why the elapsed time is slightly higher~~  
606 ~~when CAMx running with 5 parallel processes compared to 4 parallel processes as~~  
607 ~~shown in the Supplementary Material.~~

删除的内容: .

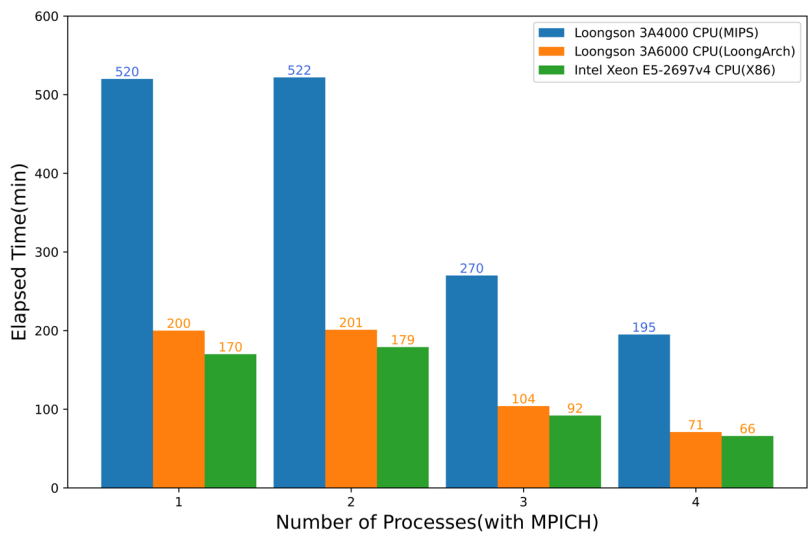
带格式的: 缩进: 首行缩进: 2 字符

删除的内容: reaches 5

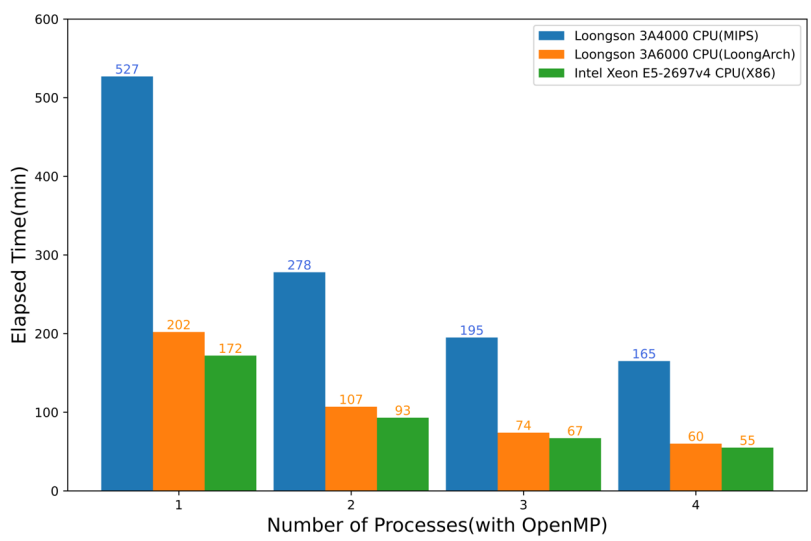
删除的内容: ↵



删除的内容:



612



613

614 **Figure 9.** Elapsed time of CAMx model running simulation case [with MPICH and](#)  
 615 [OpenMP](#) for [24](#) hours on the MIPS, [LoongArch](#) and benchmark platforms.

删除的内容: 2

616

617 In the recent years, the Longsoon CPUs have been continuously upgraded.  
 618 Compared to the previous generations of products, the performance of [Loongson CPUs](#)  
 619 [has](#) shown significant improvement. Wu et al. (2019) simulated a nested domain

删除的内容: the Longsoon 3A4000 CPU

622 covering Beijing for 48 hours using the MM5 model on the Loongson 3A quad-core  
623 CPU platform. The results showed that the computational capacity of the Loongson 3A  
624 platform for the MM5 model is approximately equivalent to around 1/12 of the Intel  
625 Core 2 Q8400 quad-core CPU, which was released in the same year. In the study of  
626 Luo et al. (2011), a comparison between Loongson 3A and Intel i5 was made by running  
627 NPB benchmark on each platform. The results shows that the performance of the 3A is  
628 nearly one-tenth of that of the i5. The rapid development of Loongson CPUs has  
629 provided a strong hardware foundation for the application of numerical simulation and  
630 scientific computing on MIPS [and LoongArch](#) architecture CPU platforms. The  
631 adaptation and optimization of the models based on [RISC](#) CPUs will also be an  
632 important research direction in the future.

删除的内容: MIPS

633

## 634 **6 Conclusion**

635 This study describes the application of the WRF-CAMx model on the MIPS CPU  
636 platform. The platform used in this study is Loongson 3A4000 quad-core CPU [with the](#)  
637 [main frequency of 1.8-2.0GHz, which can offer](#) a peak operational speed of 128GFlops.

删除的内容: 2.0GHz

删除的内容: offering

638 It is equipped with the MIPS GNU compiler. The benchmark platform used the Intel  
639 Xeon E5-2697 v4 CPU along with the same version of X86 GNU compiler. Based on  
640 the characteristics of CPU architecture and compiler, this study has successfully  
641 completed the construction of runtime environment for the WRF-CAMx modeling  
642 system. The application of an air quality modelling system based on WRF-CAMx was  
643 successfully tested using a 72-hour simulation case in the Beijing-Tianjin-Hebei region.

644 The results showed that the spatial distribution of the meteorological variables and  
645 air pollutant species was nearly identical, with relative errors in the range of  $\pm 0.1\%$ .  
646 Statistically, the maximum MAEs of major species ranged from  $10^{-3}$  to  $10^{-2}$  ppbv ( $\mu\text{g}$   
647  $\text{m}^{-3}$ ), the maximum RMSEs ranged from  $10^{-2}$  to  $10^{-1}$  ppbv ( $\mu\text{g}$   $\text{m}^{-3}$ ), and the MAPEs  
648 remained within 0.5%, that the differences caused by the architectures and compilers  
649 were within a reasonable range. Simulating a 2h-case with four parallel processes using  
650 MPICH, CAMx takes about 15.2min on Loongson 3A4000 CPU and 4.8 min on Intel

654 Xeon E5-2697 v4 CPU. In terms of single-core CPU performance, the single-core  
655 computing capability of Loongson 3A4000 CPU for the WRF-CAMx modeling system  
656 is about one-third of Intel Xeon E5-2697 v4 CPU.

657 Currently, Loongson Technology has **focused on** the LoongArch architecture and  
658 it has been used in the **latest** product. It is foreseeable that the LoongArch architecture  
659 will lead to more significant performance improvements. In the future, as the numerical  
660 models become more complex and computational scales become larger, more models  
661 will be tested on high-performance computing platforms equipped with the LoongArch  
662 architecture CPUs.

删除的内容: introduced

删除的内容: which is compatible with MIPS,

删除的内容: next-generation

删除的内容: , the 3A5000 CPU (Hu et al., 2022)

663  
664 **Code and data availability.** The source codes of CAMx version 6.10 are available at  
665 <https://camx-wp.azurewebsites.net/download/source> (ENVIRON, 2023). The datasets  
666 related to this paper and the **binary executable files of CAMx** for MIPS and LoongArch  
667 CPUs are available online via ZENODO (<https://doi.org/10.5281/zenodo.10722127>).

删除的内容: CAMx codes

删除的内容: <https://zenodo.org/records/10297970>

668  
669 **Supplement.** The supplement related to this article is available on-line.

670  
671 **Author contributions.** ZB and QW conducted the simulation and prepared the materials.  
672 QW planned and organized the project. ZB and QW completed the porting and  
673 application of the model for MIPS and LoongArch CPUs. YS collected and prepared  
674 the emission data for the simulation. ZB, QW, KC, and HC participated in the  
675 discussion.

676  
677 **Acknowledgements.** The National Key R&D Program of China (2020YFA0607804)  
678 and the Beijing Advanced Innovation Program for Land Surface funded this work. The  
679 research is supported by the High Performance Scientific Computing Center (HSCC)  
680 of Beijing Normal University.

681  
682 **Competing interests.** The contact author has declared that none of the authors has any  
683 competing interests.

690

## 691 References

- 692 Amer, A., Balaji, P., Bland, W., Gropp, W., Guo, Y., Latham, R., Lu, H., Oden, L., Pena, A. J.,  
693 Raffenetti, K., Seo, S., Si, M., Thakur, R., Zhang, J., and Zhao, X.: MPICH User's Guide  
694 Version 3.4, available at: <https://www.mpich.org/static/downloads/3.4/mpich-3.4-userguide.pdf>,  
695 2021.
- 696 Appel, K. W., Napelenok, S. L., Foley, K. M., Pye, H. O. T., Hogrefe, C., Luecken, D. J., Bash, J.  
697 O., Roselle, S. J., Pleim, J. E., Foroutan, H., Hutzell, W. T., Pouliot, G. A., Sarwar, G., Fahey, K.  
698 M., Gantt, B., Gilliam, R. C., Heath, N. K., Kang, D., Mathur, R., and Schwede, D. B.: Description  
699 and evaluation of the Community Multiscale Air Quality (CMAQ) modeling system version 5.1,  
700 Geoscientific Model Development, 10, 1703–1732, <https://doi.org/10.5194/gmd-10-1703-2017>,  
701 2017.
- 702 Appel, K. W., Bash, J. O., Fahey, K. M., Foley, K. M., Gilliam, R. C., Hogrefe, C., Hutzell, W. T.,  
703 Kang, D., Mathur, R., Murphy, B. N., Napelenok, S. L., Nolte, C. G., Pleim, J. E., Pouliot, G. A.,  
704 Pye, H. O. T., Ran, L., Roselle, S. J., Sarwar, G., Schwede, D. B., Sidi, F. I., Spero, T. L., and  
705 Wong, D. C.: The Community Multiscale Air Quality (CMAQ) model versions 5.3 and 5.3.1:  
706 system updates and evaluation, Geoscientific Model Development, 14, 2867–2897,  
707 <https://doi.org/10.5194/gmd-14-2867-2021>, 2021.
- 708 Bai, X., Tian, H., Liu, X., Wu, B., Liu, S., Hao, Y., Luo, L., Liu, W., Zhao, S., Lin, S., Hao, J., Guo,  
709 Z., and Lv, Y.: Spatial-temporal variation characteristics of air pollution and apportionment of  
710 contributions by different sources in Shanxi province of China, Atmospheric Environment, 244,  
711 117926, <https://doi.org/10.1016/j.atmosenv.2020.117926>, 2021.
- 712 Cao, K., Wu, Q., Wang, L., Wang, N., Cheng, H., Tang, X., Li, D., and Wang, L.: GPU-HADVPPM  
713 V1.0: a high-efficiency parallel GPU design of the piecewise parabolic method (PPM) for  
714 horizontal advection in an air quality model (CAMx V6.10), Geosci. Model Dev., 16, 4367–4383,  
715 <https://doi.org/10.5194/gmd-16-4367-2023>, 2023.
- 716 Chen, H. S., Wang, Z. F., Li, J., Tang, X., Ge, B. Z., Wu, X. L., Wild, O., and Carmichael, G. R.:  
717 GNAQPMS-Hg v1.0, a global nested atmospheric mercury transport model: model description,  
718 evaluation and application to trans-boundary transport of Chinese anthropogenic emissions,  
719 Geoscientific Model Development, 8, 2857–2876, <https://doi.org/10.5194/gmd-8-2857-2015>,  
720 2015.
- 721 George, A. D.: An overview of RISC vs. CISC, in: [1990] Proceedings. The Twenty-Second  
722 Southeastern Symposium on System Theory, The Twenty-Second Southeastern Symposium on  
723 System Theory, Cookeville, TN, USA, 436–438, <https://doi.org/10.1109/SSST.1990.138185>,  
724 1990.
- 725 Hennessy, J., Jouppi, N., Przybylski, S., Rowen, C., Gross, T., Baskett, F., and Gill, J.: MIPS: A  
726 microprocessor architecture, SIGMICRO Newsl., 13, 17–22,  
727 <https://doi.org/10.1145/1014194.800930>, 1982.
- 728 Hu, W., Wang, J., Gao, X., Chen, Y., Liu, Q., and Li, G.: Godson-3: A Scalable Multicore RISC  
729 Processor with x86 Emulation, IEEE Micro, 29, 17–29, <https://doi.org/10.1109/MM.2009.30>,  
730 2009.
- 731 Hu, W., Zhang, Y., and Fu, J.: An introduction to CPU and DSP design in China, Sci. China Inf. Sci.,  
732 59, 1–8, <https://doi.org/10.1007/s11432-015-5431-6>, 2016.

删除的内容: Guo, L. and Liu, Y.: Efficient Implementation of FFT on Loongson 3A CPU, Journal of Chinese Computer Systems, 33, 594–597, 2012 (in Chinese).<sup>4</sup>

736 Hu, W., Gao, X., and Zhang, G.: Building the software ecosystem for the Loongson instruction set  
737 architecture, *Information and Communications Technology and Policy*, 43–48, 2022 (in Chinese).

738 Hu, W.-W., Gao, Y.-P., Chen, T.-S., and Xiao, J.-H.: The Godson Processors: Its Research,  
739 Development, and Contributions, *J. Comput. Sci. Technol.*, 26, 363–372,  
740 <https://doi.org/10.1007/s11390-011-1139-2>, 2011.

741 Intel Inc.: Intel® 64 and IA-32 Architectures Software Developer’s Manual, Volume 1: Ba  
742 sic Architecture, available at: [https://www.intel.com/content/www/us/en/developer/articles/te  
743 chnical/intel-sdm.html](https://www.intel.com/content/www/us/en/developer/articles/technical/intel-sdm.html), 2023.

744 Li, L., Chen, Z., and Wang, S.: Power Consumption and Analysis of Server Based on Loongson  
745 CPU No. 3, *Information Technology & Standardization*, 46–50, 2014 (in Chinese).

746 Liu, Y., Ye, K., and Xu, C.-Z.: Performance Evaluation of Various RISC Processor Systems: A Case  
747 Study on ARM, MIPS and RISC-V, in: *Cloud Computing – CLOUD 2021*, Cham, 61–74,  
748 [https://doi.org/10.1007/978-3-030-96326-2\\_5](https://doi.org/10.1007/978-3-030-96326-2_5), 2022.

749 Luo, Q., Kong, C., Cai, Y., and Liu, G.: Performance Evaluation of OpenMP Constructs and Kernel  
750 Benchmarks on a Loongson-3A Quad-Core SMP System, in: *2011 12th International Conference  
751 on Parallel and Distributed Computing, Applications and Technologies, 2011 12th International  
752 Conference on Parallel and Distributed Computing, Applications and Technologies*, 191–196,  
753 <https://doi.org/10.1109/PDCAT.2011.66>, 2011.

754 Mallach, E. G.: RISC: Evaluation and Selection, *Journal of Information Systems Management*, 8,  
755 8–16, <https://doi.org/10.1080/07399019108964978>, 1991.

756 Michalakes, J., Chen, S., Dudhia, J., Hart, L., Klemp, J., Middlecoff, J., and Skamarock, W.:  
757 Development of a next-generation regional weather research and forecast model, in:  
758 *Developments in Teracomputing*, WORLD SCIENTIFIC, 269–276,  
759 [https://doi.org/10.1142/9789812799685\\_0024](https://doi.org/10.1142/9789812799685_0024), 2001.

760 MIPS Technology Inc.: MIPS Architecture For Programmers Volume I-A, available at:  
761 <https://www.mips.com/products/architectures/mips64>, 2014.

762 Pepe, N., Pirovano, G., Lonati, G., Balzarini, A., Toppetti, A., Riva, G. M., and Bedogni, M.:  
763 Development and application of a high resolution hybrid modelling system for the evaluation of  
764 urban air quality, *Atmospheric Environment*, 141, 297–311,  
765 <https://doi.org/10.1016/j.atmosenv.2016.06.071>, 2016.

766 Powers, J. G., Klemp, J. B., Skamarock, W. C., Davis, C. A., Dudhia, J., Gill, D. O., Coen, J. L.,  
767 Gochis, D. J., Ahmadov, R., Peckham, S. E., Grell, G. A., Michalakes, J., Trahan, S., Benjamin,  
768 S. G., Alexander, C. R., Dimego, G. J., Wang, W., Schwartz, C. S., Romine, G. S., Liu, Z., Snyder,  
769 C., Chen, F., Barlage, M. J., Yu, W., and Duda, M. G.: *The Weather Research and Forecasting  
770 Model: Overview, System Efforts, and Future Directions*, *Bulletin of the American  
771 Meteorological Society*, 98, 1717–1737, <https://doi.org/10.1175/BAMS-D-15-00308.1>, 2017.

772 RAMBOLL ENVIRON Inc.: CAMx User’s Guide Version 6.1, available at: [https://camx-  
773 wp.azurewebsites.net/Files/CAMxUsersGuide\\_v6.10.pdf](https://camx-wp.azurewebsites.net/Files/CAMxUsersGuide_v6.10.pdf), 2014.

774 Shi, Z.: Technology comparison and research of RISC and CISC, *China Science and Technology  
775 Information*, 131–132, 2008 (in Chinese).

776 Skamarock, C., Klemp, B., Dudhia, J., Gill, O., Liu, Z., Berner, J., Wang, W., Powers, G., Duda, G.,  
777 Barker, D., and Huang, X.: A Description of the Advanced Research WRF Model Version 4,  
778 <https://doi.org/10.5065/1dfh-6p97>, 2019.

779 Sun Y.: Research on the contribution of soil fugitive dust in Beijing based on satellite identification

删除的内容: Li, L., Chen, Y.-J., Liu, D.-F., Qian, C., and  
Hu, W.-W.: An FFT Performance Model for Optimizing  
General-Purpose Processor Architecture, *J. Comput. Sci.  
Technol.*, 26, 875–889, [https://doi.org/10.1007/s11390-011-  
0186-z](https://doi.org/10.1007/s11390-011-0186-z), 2011. <sup>d</sup>

785 and numerical simulation technology, Master, Beijing Normal University, <https://etdlib.bnu.edu.cn>,  
786 2022a.

787 Sun, Y., Wu, Q., Wang, L., Zhang, B., Yan, P., Wang, L., Cheng, H., Lv, M., Wang, N., and Ma, S.:  
788 Weather Reduced the Annual Heavy Pollution Days after 2016 in Beijing, *Sola*, 18, 135–139,  
789 <https://doi.org/10.2151/sola.2022-022>, 2022b.

790 The HDF Group: HDF5 User's Guide Version 1.1, available at:  
791 <https://portal.hdfgroup.org/display/HDF5/HDF5+User+Guides>, 2019.

792 UCAR/Unidata: NetCDF User's Guide Version 1.1, available at: <https://docs.unidata.ucar.edu/nug>,  
793 2021.

794 Wang, K., Gao, C., Wu, K., Liu, K., Wang, H., Dan, M., Ji, X., and Tong, Q.: ISAT v2.0: an  
795 integrated tool for nested-domain configurations and model-ready emission inventories for WRF-  
796 AQM, *Geoscientific Model Development*, 16, 1961–1973, [https://doi.org/10.5194/gmd-16-1961-](https://doi.org/10.5194/gmd-16-1961-2023)  
797 [2023](https://doi.org/10.5194/gmd-16-1961-2023), 2023.

798 Wang, P., Jiang, J., Lin, P., Ding, M., Wei, J., Zhang, F., Zhao, L., Li, Y., Yu, Z., Zheng, W., Yu, Y.,  
799 Chi, X., and Liu, H.: The GPU version of LASG/IAP Climate System Ocean Model version 3  
800 (LICOM3) under the heterogeneous-compute interface for portability (HIP) framework and its  
801 large-scale application, *Geosci. Model Dev.*, 14, 2781–2799, [https://doi.org/10.5194/gmd-14-](https://doi.org/10.5194/gmd-14-2781-2021)  
802 [2781-2021](https://doi.org/10.5194/gmd-14-2781-2021), 2021.

803 Wang, S., Li, L., and Chen, Z.: The Test and Analysis on Memory Access Performance Based on  
804 Loongson CPU, *Information Technology & Standardization*, 32–36, 2014 (in Chinese).

805 Wang, Z., Xie, F., Wang, X., An, J., and Zhu, J.: Development and Application of Nested Air Quality  
806 Prediction Modeling System, *Chinese Journal of Atmospheric Sciences*, 778–790,  
807 <http://dx.doi.org/10.3878/j.issn.1006-9895.2006.05.07>, 2006.

808 Wu, Q. and Cheng, H.: Transplantation and application of mesoscale mode on Loongson CPU  
809 platform, *Journal of Beijing Normal University (Natural Science)*, 55, 11–18,  
810 <https://doi.org/10.16360/j.cnki.jbnuns.2019.01.002>, 2019.

811 Wu, Q., Xu, W., Shi, A., Li, Y., Zhao, X., Wang, Z., Li, J., and Wang, L.: Air quality forecast of  
812 PM10 in Beijing with Community Multi-scale Air Quality Modeling (CMAQ) system: emission  
813 and improvement, *Geoscientific Model Development*, 7, 2243–2259,  
814 <https://doi.org/10.5194/gmd-7-2243-2014>, 2014.

815 Wu, Y., Xu, G., Zhao, Y., and Tan, Y.: Parallel Processing on WRF Meteorological Data Using  
816 MPICH, in: 2012 Sixth International Conference on Internet Computing for Science and  
817 Engineering, 2012 Sixth International Conference on Internet Computing for Science and  
818 Engineering, titleTranslation., 262–265, <https://doi.org/10.1109/ICICSE.2012.12>, 2012.

819 Xiao, H., Wu, Q., Yang, X., Wang, L., and Cheng, H.: Numerical study of the effects of initial  
820 conditions and emissions on PM2.5 concentration simulations with CAMx v6.1: a Xi'an case  
821 study, *Geoscientific Model Development*, 14, 223–238, [https://doi.org/10.5194/gmd-14-223-](https://doi.org/10.5194/gmd-14-223-2021)  
822 [2021](https://doi.org/10.5194/gmd-14-223-2021), 2021.

823 Yang, X., Xiao, H., Wu, Q., Wang, L., Guo, Q., Cheng, H., Wang, R., and Tang, Z.: Numerical study  
824 of air pollution over a typical basin topography: Source appointment of fine particulate matter  
825 during one severe haze in the megacity Xi'an, *Science of The Total Environment*, 708, 135213,  
826 <https://doi.org/10.1016/j.scitotenv.2019.135213>, 2020.

827 Zhang, Y., Bocquet, M., Mallet, V., Seigneur, C., and Baklanov, A.: Real-time air quality forecasting,  
828 part I: History, techniques, and current status, *Atmospheric Environment*, 60, 632–655,

829 <https://doi.org/10.1016/j.atmosenv.2012.06.031>, 2012.  
830 Zhang, Z., Wang, X., Cheng, S., Guan, P., Zhang, H., Shan, C., and Fu, Y.: Investigation on the  
831 difference of PM<sub>2.5</sub> transport flux between the North China Plain and the Sichuan Basin,  
832 Atmospheric Environment, 271, 118922, <https://doi.org/10.1016/j.atmosenv.2021.118922>, 2022.  
833 Zhen, J., Guan, P., Yang, R., and Zhai, M.: Transport matrix of PM<sub>2.5</sub> in Beijing-Tianjin-Hebei and  
834 Yangtze River Delta regions: Assessing the contributions from emission reduction and  
835 meteorological conditions, Atmospheric Environment, 304, 119775,  
836 <https://doi.org/10.1016/j.atmosenv.2023.119775>, 2023.  
837 Zhi, Y. and Xu, J.: Android transplantation and analysis based on Loongson, in: 2012 International  
838 Conference on Information Management, Innovation Management and Industrial Engineering,  
839 2012 International Conference on Information Management, Innovation Management and  
840 Industrial Engineering, 59–61, <https://doi.org/10.1109/ICIII.2012.6339777>, 2012.

删除的内容: Zhao, M., Zhang, Y., Liu, Y., Li, Y., and Yan, S.: Comparison and Analysis of Three Types of FFT Adaptive Libraries on Loongson 3A, Computer Science, 39, 281–285, 2012 (in Chinese).<sup>4</sup>



第 10 页: [1] 删除的内容

Zehua Bai

2024/2/28 03:22:00

第 11 页: [2] 删除的内容

Zehua Bai

2024/2/28 03:33:00

第 12 页: [3] 删除的内容

Zehua Bai

2024/2/28 03:50:00